Exact gauge invariant mass dependence of α_s through two loops

Michael Melles[a*]

[a]Department of Physics,
Durham University,
Durham, DH1 3LE, U.K.

A physically defined QCD coupling parameter naturally incorporates massive quark flavor thresholds in a gauge invariant, renormalization scale independent and analytical way. In this paper we summarize recent results for the finite-mass fermionic corrections to the heavy quark potential through two loops leading to the numerical solution of the physical and mass dependent Gell-Mann Low function. The decoupling-, massless- and Abelian-limits are reproduced and an analytical fitting function is obtained in the V-scheme. Thus the gauge invariant mass dependence of α_V is now known through two loops. Possible applications in lattice analyses, heavy quark physics and effective charges are briefly discussed.

1. Introduction

Quark flavor thresholds in QCD are commonly treated within effective descriptions in MS-like coupling definitions by imposing matching conditions at the quark thresholds [1,2]. Thus quarks are considered infinitely heavy below and massless above m_q and the coupling is non-analytic at the thresholds. Real mass effects need to be calculated separately as higher twist effects in the small and large mass limits. For the intermediate range an all orders resummation of these expansions is necessary. In this paper we summarize recent results presented in Refs. [3,4] based on a physical coupling definition obtained from the static quark-antiquark potential [5], $V(Q^2,m^2) \equiv -4\pi C_F \frac{\alpha_V(Q^2,m^2)}{Q^2}$, which naturally incorporates massive quarks and where the scale $Q^2 \equiv -q^2 = \mathbf{q^2}$ is identified with exchanged momentum between the heavy sources. A technical complication is that the massive Gell-Mann Low function can only be solved numerically due to the complexity of the obtained results and that it is scheme dependent already at one loop. The latter point can be ameliorated by expressing other physical charges through α_V and using the conformal ansatz [4]. We begin in the next section by reviewing the two-loop corrections including massive quarks to $V(Q^2,m^2)$ and then discuss the solutions to the massive renormalization group equations. Finally we briefly outline possible applications.

*Research supported by the EU Fourth Framework Programme 'Training and Mobility of Researchers' through a Marie Curie Fellowship.

2. Two loop corrections

The results obtained in Ref. [3] express the physical charge α_V in the MS-scheme, which is used as a calculational tool, in the following way:

$$\alpha_V(Q,m) = \alpha_{\rm MS}(\mu)\left(1 + v_1(Q,m(\mu),\mu)\frac{\alpha_{\rm MS}(\mu)}{\pi} + v_2(Q,m(\mu),\mu)\frac{\alpha^2_{\rm MS}(\mu)}{\pi^2} + \cdots\right) \quad (1)$$

where v_2 contains the diagrams of Fig. 1 and the MS-counterterms displayed in Fig. 2. A strong check of the results in Ref. [3] is given by the successful reproduction of the fermionic gluon wave function renormalization constant (RC) and the locality of all other RC's as these are mass independent in minimally subtracted schemes.

For the heavier quark masses m_c, m_b and m_t the pole-mass definition is suitable and allows for a straightforward Abelian limit as well as the renormalization scale independence of the Gell-Mann Low function below. The next-to-leading

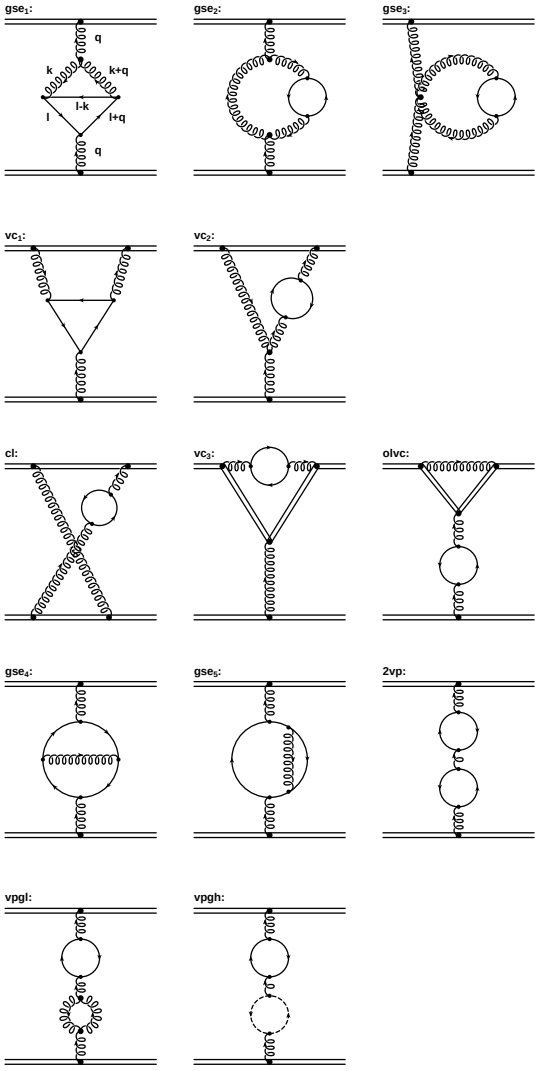

Figure 1. The massive fermionic corrections to the heavy quark potential through two loops in the Feynman gauge. The straight ladder diagram does not contribute as it is already contained in the iteration of lower order amplitudes. The middle line contains IR-divergent diagrams, however, their sum is IR-finite. Contributions proportional to C_F and C_A are separately gauge invariant for α_V. After inclusion of the counterterms in Fig. 2 the correct massless limit given in Refs. [6,7] is obtained. Details can be found in Ref. [3].

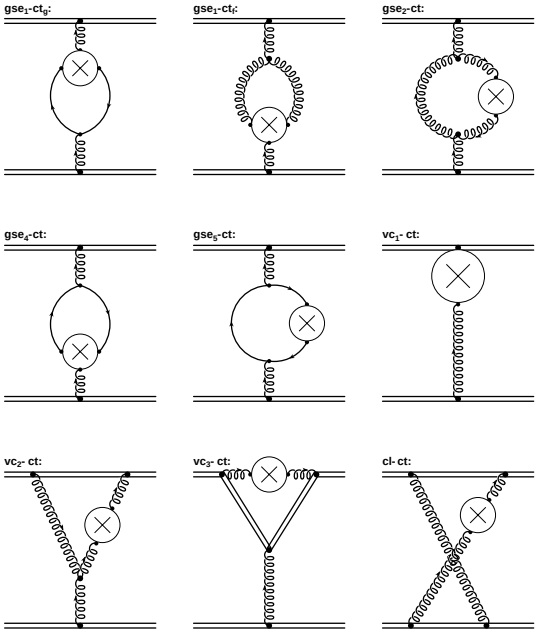

Figure 2. The two loop counterterms corresponding to the diagrams in Fig. 1. Adding these contributions to the original graphs removes all non-local functions from the occurring pole terms. The only exception are $\frac{m^2}{\epsilon}$ terms in the two point functions which only cancel in the sum of all two point diagrams. The fact that the tadpole diagram has no counterterm is already indicative of this cancellation.

order relation between the MS mass $m(\mu)$ and the pole mass m is given by [8]:

$$m(\mu) = m\left[1 - C_F\frac{\alpha_{\rm MS}(\mu)}{\pi}\left(1 + \frac{3}{2}\log\frac{\mu}{m} - \frac{3}{4}\left[\gamma - \log(4\pi)\right]\right)\right] \quad (2)$$

where γ is the Euler constant. Inserting Eq. (2) into Eq. (1) gives at next-to-next-to-leading order

$$\alpha_V(Q,m) = \alpha_{\rm MS}(\mu)\left[1 + v_1(Q,m,\mu)\frac{\alpha_{\rm MS}(\mu)}{\pi} + \left[v_2(Q,m,\mu) + \Delta_m(Q,m,\mu)\right]\frac{\alpha_{\rm MS}^2(\mu)}{\pi^2}\right] \quad (3)$$

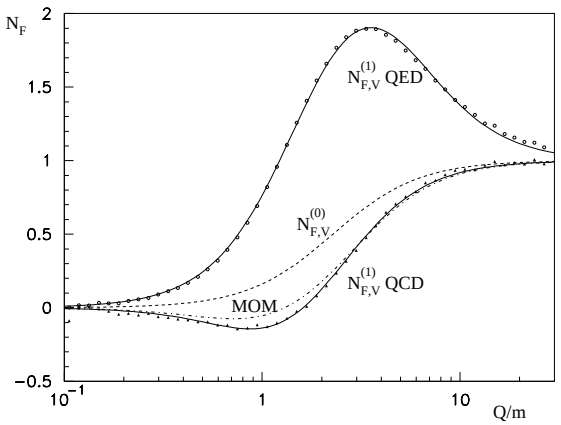

Figure 3. The numerical results for the gauge-invariant $N^{(1)}_{F,V}$ in QED (open circles) and QCD (triangles) with the best χ^2 fits of Eqs. (10) and (9) superimposed respectively. The dashed line shows the one-loop $N^{(0)}_{F,V}$ function. For comparison we also show the gauge dependent two-loop result obtained in MOM schemes (dash-dot) [10,11]. At large $\frac{Q}{m}$ the theory becomes effectively massless, and both schemes agree as expected. The figure also illustrates the decoupling of heavy quarks at small $\frac{Q}{m}$.

where $\Delta_m(Q,m,\mu)$ denotes the contribution arising from v_1 when changing from the MS mass to the pole mass.

3. Numerical solutions of the Gell-Mann Low function

The Gell-Mann Low function [12] for the V-scheme is defined as the total logarithmic derivative of the effective charge with respect to the physical momentum transfer scale Q:

$$\Psi_V\left(\frac{Q}{m}\right) \equiv \frac{d\alpha_V(Q,m)}{d\log Q} \equiv \sum_{i=0}^{\infty} -\psi_V^{(i)} \frac{\alpha_V^{i+2}(Q,m)}{\pi^{i+1}} \quad (4)$$

For the massive case all the mass effects will be collected into a mass-dependent function N_F. In other words we will write

$$\psi_V^{(0)}\left(\frac{Q}{m}\right) = \frac{11}{2} - \frac{1}{3} N_{F,V}^{(0)}\left(\frac{Q}{m}\right) \quad (5)$$

$$\psi_V^{(1)}\left(\frac{Q}{m}\right) = \frac{51}{4} - \frac{19}{12} N_{F,V}^{(1)}\left(\frac{Q}{m}\right) \quad (6)$$

where the subscript V indicates the scheme dependence of $N^{(0)}_{F,V}$ and $N^{(1)}_{F,V}$.

Taking the derivative of Eq. (3) with respect to $\log Q$ and re-expanding the result in $\alpha_V(Q,m)$ gives the following equations for the first two coefficients of Ψ_V:

$$\psi_V^{(0)}\left(\frac{Q}{m}\right) = -\frac{dv_1(Q,m,\mu)}{d\log Q} \quad (7)$$

$$\psi_V^{(1)}\left(\frac{Q}{m}\right) = -\frac{d[v_2(Q,m,\mu)+\Delta_m(Q,m,\mu)]}{d\log Q} + 2v_1(Q,m,\mu)\frac{dv_1(Q,m,\mu)}{d\log Q} \quad (8)$$

The argument Q/m indicates that there is no renormalization-scale dependence in Eqs. (7) and (8). Rather, $\psi_V^{(0)}$ and $\psi_V^{(1)}$ are functions of the ratio of the physical momentum transfer $Q=\sqrt{-q^2}$ and the pole mass m only. A numerical solution based on the MC-integrator VEGAS and numerical differentiation gives stable results summarized in Fig. 3. In the case of QCD we obtain the following approximate form for the effective number of flavors for a given quark with mass m [4]:

$$N_{F,V}^{(1)}\left(\frac{Q}{m}\right) \approx \frac{\left(-0.571+0.221\frac{Q^2}{m^2}\right)\frac{Q^2}{m^2}}{1+1.326\frac{Q^2}{m^2}+0.221\frac{Q^4}{m^4}} \quad (9)$$

and for QED

$$N_{F,V}^{(1)}\left(\frac{Q}{m}\right) \approx \frac{\left(1.069+0.0133\frac{Q^2}{m^2}\right)\frac{Q^2}{m^2}}{1+0.402\frac{Q^2}{m^2}+0.0133\frac{Q^4}{m^4}} \quad (10)$$

The results of our numerical calculation of $N^{(1)}_{F,V}$ in the V-scheme for QCD and QED are shown in Fig. 3. The decoupling of heavy quarks becomes manifest at small Q/m, and the massless limit is attained for large Q/m.

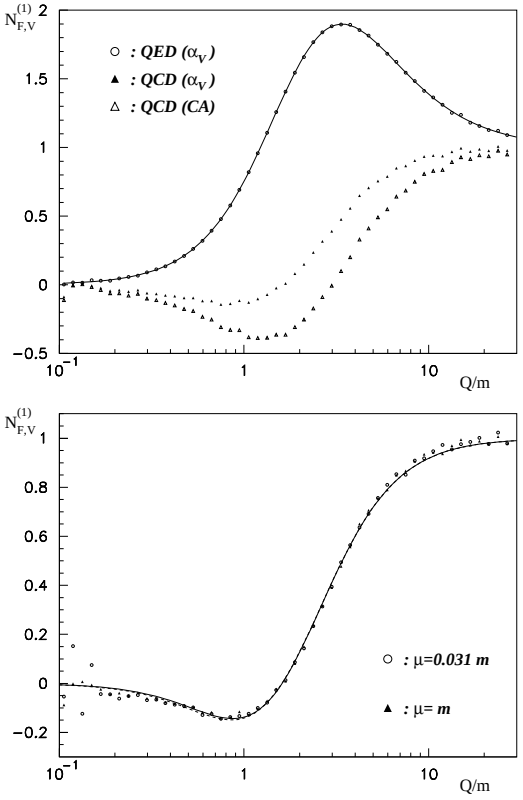

Figure 4. The upper diagram displays a comparison of the Abelian limit of our results (open circles) for $N^{(1)}_{F,V}$ based on the calculation in Ref. [3] which was done in the MS-scheme with the well known result in the literature [9] done in the on-shell renormalization scheme (solid line). Also shown are the gauge invariant non-Abelian contribution only ($\propto C_A$) (open triangles) as well as the sum of all terms in QCD (solid triangles). The correct Abelian behavior is a very strong check on the results given in Ref. [3]. The lower diagram illustrates the renormalization scale independence of the two-loop effective number of flavors $N^{(1)}_{F,V}$ as a function of the ratio of the physical momentum transfer Q over the pole mass m. Numerical instabilities are visible for small values of $\frac{Q}{m}$ and occur because of limited Monte Carlo statistics (10^7 evaluations for each of the 50 iterations). The two fits obtained, which agree within statistical errors, are shown as a solid and dashed line for $\mu = m$ and $\mu = 0.031m$ respectively.

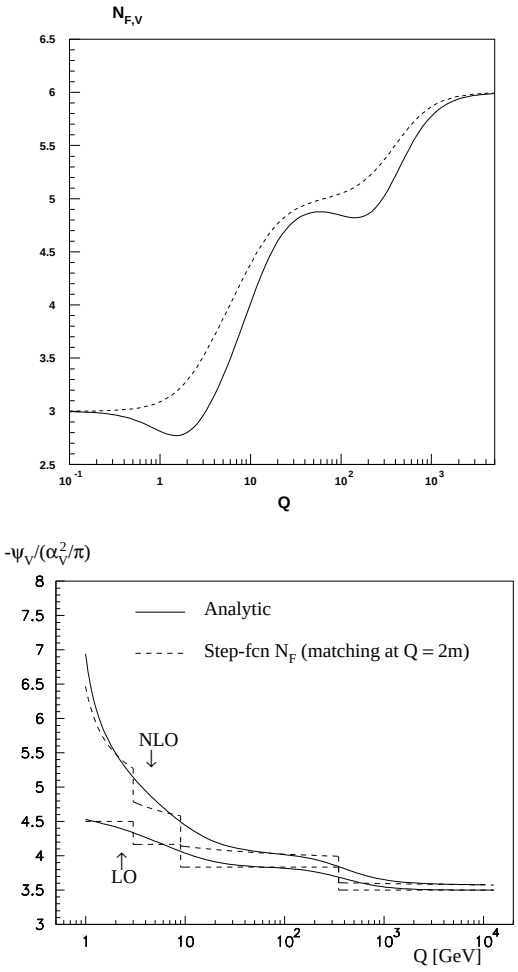

Figure 5. The upper plot shows the sum of the effective number of flavors for one (dashed line) and two loops in the V-scheme. We use quark pole masses with $m_c = 1.5$GeV, $m_b = 4.5$GeV and $m_t = 173$GeV. The two loop $N^{(1)}_{F,V}$ starts to decrease from the fixed starting point $N_{F,V} = 3$ due to the novel non-Abelian anti screening corrections and then increases more rapidly as the one loop $N^{(0)}_{F,V}$. Below 1TeV, there is no regime for which the quark masses can be neglected. The lower plot displays the scaled Ψ-function, $-\Psi_V/(\alpha_V^2/\pi)$ in the analytic V-scheme $\alpha_V(Q, m_i)$ (solid) compared to the $\alpha_V(Q, \Theta)$ scheme with discrete theta-function treatment of flavor thresholds with continuous matching at $Q = m$ (dashed).

We can also apply the same fitting procedure to the dependence of the one-loop effective $N_{F,V}^{(0)} \approx \frac{1}{1+5.19\frac{m^2}{Q^2}}$. Fig. 4 demonstrates that the new non-Abelian contributions ($\sim C_A$) are responsible for the negative $N_{F,V}^{(1)}$ at intermediate Q/m due to anti-screening. The Abelian corrections on the other hand are larger than 1 in this regime and agree with the literature results obtained in the on-shell scheme [9]. In addition the lower graph of Fig. 4 demonstrates the renormalization scale independence of the solution to the Gell-Mann Low function.

Fig. 5 demonstrates the smoothness and analyticity of the renormalization group solutions and compares the massive results with the massless ones including one-loop matching at the two loop order. The figure demonstrates that there is really no regime below 1 TeV where quarks can be considered massless for running coupling effects in the V-scheme.

4. Conclusions

In summary, we have presented the gauge invariant mass dependence of α_s through two loops in the physically motivated V-scheme. The result was shown to posses the correct massless limit and gives automatic decoupling of heavy quarks. In addition the correct Abelian limit is reproduced and the renormalization scale independent results can be parameterized by a simple analytical fitting function. Non-Abelian anti-screening effects lead to a negative number of flavors for intermediate energies at the two loop level.

Massive renormalization group solutions are scheme dependent already at one-loop, however, the mass dependence of α_V can be transferred to other physical charges through commensurate scale relations [13]. In Ref. [4] this was done for the non-singlet hadronic width of the Z-boson and compared with the $\overline{MS}$-scheme higher twist corrections. For perturbative energies a persistent $\sim$1% deviation was observed which characterizes the residual scheme dependence of the two loop predictions for this observable. In a similar way, all other effective charges can be described.

Other possible applications include the effect of a massive charm on the bottom mass determination. Here massive charm corrections to the potential and in the running coupling could potentially lead to a shift in the bottom mass of $\mathcal{O}\left(m_c\alpha_s^2(m_b)\right)$ and thus would need to be included into a proper analysis. Also top quark physics at the NLC could provide fruitful ground for a V-scheme analysis.

A further interesting comparison could be performed with lattice analyses investigating the transition region of perturbative and non-perturbative regimes. For this purpose the Fourier transform $\alpha_V(1/r) = \int \frac{d^3q}{(2\pi)^3}\alpha_V(q^2,m^2)$ or $\alpha_{q,\overline{q}}(r) \equiv -r^2\frac{\partial V(1/r)}{\partial r}$ must be obtained.

Acknowledgments

I would like to thank my collaborators S.J. Brodsky and J. Rathsman for their contributions to the results presented here.

REFERENCES

1. W. Bernreuther, W. Wetzel, Nucl.Phys.B 197, 228 (1982).
2. W.J. Marciano, Phys.Rev.D 29, 580 (1984).
3. M. Melles, hep-ph/9805216, Phys.Rev.D 58:114004 (1998).
4. S.J. Brodsky, M. Melles, J. Rathsman, hep-ph/9906324.
5. L. Susskind, lectures given at Les Houches 1976, North Holland 1977, 207-308.
6. M. Peter, Phys.Rev.Lett. 78, 602 (1997); Nucl.Phys.B 501, 471 (1997).
7. Y.Schröder, hep-ph/9812205.
8. R. Tarrach, Nucl.Phys.B 183, 384 (1981).
9. G. Källen, A. Sabry, Dan.Mat.Fys.Medd. 29, No. 17 (1955).
10. T. Yoshino, K. Hagiwara, Z.Phys.C 24, 185 (1984).
11. F. Jegerlehner, O.V. Tarasov, hep-ph/9809485.
12. M. Gell-Mann, F.E. Low, Phys.Rev. 95, 1300 (1954).
13. S.J. Brodsky, H.J. Lu, Phys.Rev.D 51, 3652 (1995).

gse_1-ct_g:

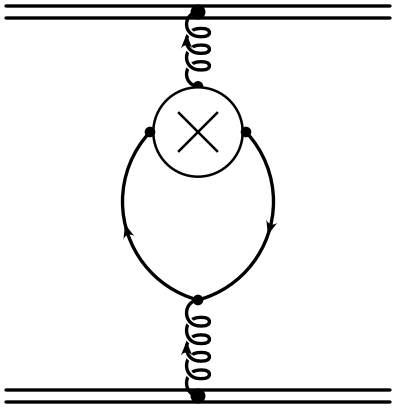

gse_1-ct_f:

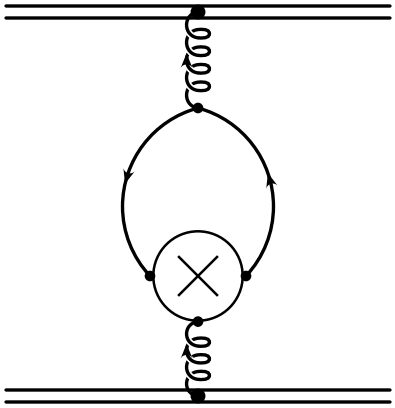

gse_2-ct:

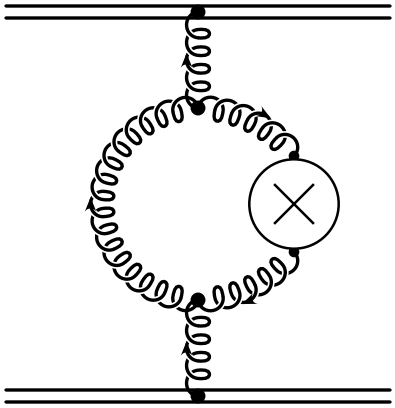

vc_1- ct:

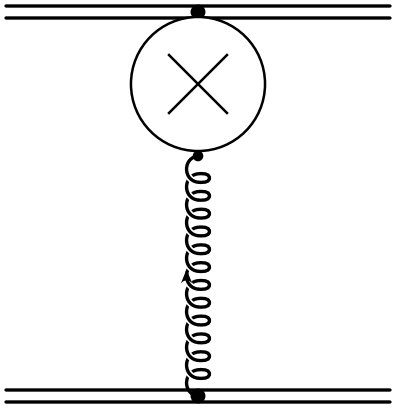

vc_2- ct:

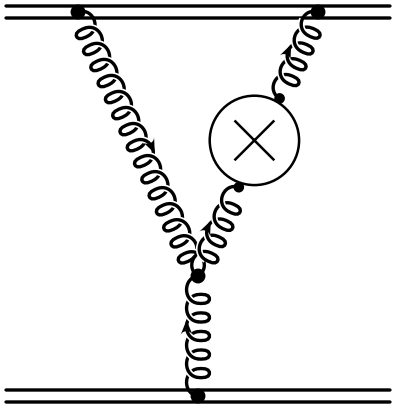

cl- ct: